

SCIENTIFIC REPORTS



OPEN

UPLC-PDA-QTOFMS-guided isolation of prenylated xanthenes and benzoylphloroglucinols from the leaves of *Garcinia oblongifolia* and their migration-inhibitory activity

Hong Zhang^{1,2,*}, Dan Zheng^{1,*}, Zhi-Jie Ding¹, Yuan-Zhi Lao^{1,2}, Hong-Sheng Tan^{1,2} & Hong-Xi Xu^{1,2}

Received: 11 July 2016

Accepted: 04 October 2016

Published: 21 October 2016

A UPLC-PDA-QTOFMS-guided isolation strategy was employed to screen and track potentially new compounds from *Garcinia oblongifolia*. As a result, two new prenylated xanthenes, oblongixanthenes D and E (1–2), six new prenylated benzoylphloroglucinol derivatives, oblongifolins V–Z (3–7) and oblongifolin AA (8), as well as a known compound oblongifolin L (9), were isolated from the EtOAc-soluble fraction of an acetone extract of the leaves of *Garcinia oblongifolia* guided by UPLC-PDA-QTOFMS analysis. The structures of the new compounds were elucidated by 1D- and 2D-NMR spectroscopic analysis and mass spectrometry. Experimental and calculated ECD spectra were used to determine the absolute configurations. The results of wound healing and transwell migration assay showed that oblongixanthenes D (1), E (2), and oblongifolin L (9) have the ability to inhibit cancer cell migration in lower cytotoxic concentrations. Western blotting results showed that these compounds exhibited an anti-metastasis effect mainly through downregulating RAF protein levels. In addition, 2 and 9 could inhibit phospho-MEK and phospho-ERK at downstream. Moreover, 1, 2, and 9 could inhibit snail protein level, suggesting that they could regulate the EMT pathway.

Garcinia oblongifolia Champ. ex Benth. (Clusiaceae), a tree or medium-sized shrub with edible fruits, is widely distributed in tropical regions of southern mainland China and northern Vietnam. It has been used for many years as a folk medicine in China to treat stomatitis, eczema, and burns^{1,2}. Previous phytochemical studies of this species led to the discovery of many new compounds, including prenylated benzoylphloroglucinols^{3–6}, xanthenes^{4,5}, biphenyls², and a new bixanthone derivative, garciobioxanthone⁷, which have been reported to possess a wide range of biological activities, including antitumor^{1,8–10}, anti-inflammatory¹¹, and antienteroviral effects^{3,12}.

In our previous study, a series of new prenylated benzoylphloroglucinols, oblongifolins J–U were isolated from the bioactive petroleum ether-soluble part of the acetone extract of *G. oblongifolia* leaves by bioassay-guided fractionation, in which two compounds exhibited significant anti-EV71 activity³. In our efforts to identify more new bioactive compounds from *Garcinia* species, the EtOAc-soluble fraction of the acetone extract of the leaves of *G. oblongifolia* was found to contain many potentially new compounds by UPLC-PDA-QTOFMS analysis. In follow-up work, UPLC-PDA-QTOFMS-guided fractionation led to the isolation of two new prenylated xanthenes, oblongixanthenes D and E (1–2), six new prenylated benzoylphloroglucinol derivatives, oblongifolins V–Z (3–7) and oblongifolin AA (8), as well as a known compound, oblongifolin L (9) from this fraction (Fig. 1).

¹School of Pharmacy, Shanghai University of Traditional Chinese Medicine, Shanghai, 201203, P.R. China.

²Engineering Research Centre of Shanghai Colleges for TCM New Drug Discovery, Shanghai, 201203, P.R. China.

*These authors contributed equally to this work. Correspondence and requests for materials should be addressed to H.-X.X. (email: xuhongxi88@gmail.com)

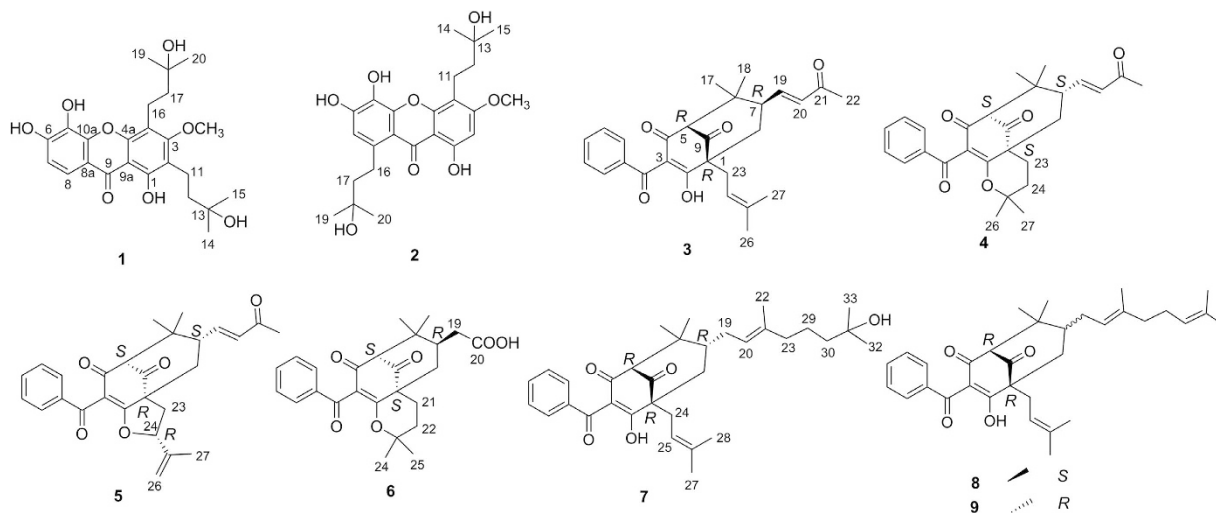


Figure 1. Compounds isolated from the leaves of *G. oblongifolia*.

In this report, the isolation and structural elucidation of these compounds, as well as their migration-inhibitory activity in esophageal cancer are described.

Results and Discussion

The EtOAc-soluble fraction of the acetone extract of the leaves of *Garcinia oblongifolia* and its subfractions were analyzed by UPLC-PDA-QTOFMS in positive mode to screen and characterize potentially new compounds. As a result, 13 unknowns of interest were detected from this extract and its subfractions by analysis of their UV, MS, and MS/MS spectra (Figures S1–S13, Supplementary information). Compounds **1** and **2** both showed the molecular ion $[M + H]^+$ at m/z 447, corresponding to a molecular formula of $C_{24}H_{30}O_8$. Their UV spectra showed similar absorption bands at approximately 257 and 327 nm, indicating that they might be xanthone derivatives (Figures S1 and S2)¹³. Compounds **3–8** and **P10–P14** produce the characteristic fragment ion at m/z 165.0182 or 177.0182 in their MS/MS spectra (Figures S3–S13), indicating that they might be polycyclic polyprenylated acylphloroglucinols (PPAPs)^{14–16}. Their molecular formulas were obtained by accurate mass measurements for precursor ions. These 13 compounds were searched using the molecular formula and further refined by their skeletons in the SciFinder database. The results indicated that they were potentially new xanthenes or PPAPs. Thus, they were selected as the targets of interest to be subjected to further phytochemical isolation. Finally, 8 new compounds (**1–8**) were isolated by column chromatography over MCI gel, silica gel, reversed-phase C_{18} silica gel, Sephadex LH-20, and preparative HPLC guided by UPLC-PDA-QTOFMS analysis. Other five potentially new PPAPs (**P10–P14**) could not be obtained, which were decomposed or oxidized during the isolation procedure or the NMR experiments. In addition, a known compound was obtained, which could be unambiguously identified as oblongifloin L (**9**) by comparison of the retention time (RT) and MS/MS data with those of the reference compound. Structural elucidation of the new compounds was achieved by HRMS, 1H NMR, ^{13}C NMR, DEPT, HSQC, HMBC, and NOSEY analyses.

Structural elucidation. Oblongixanthone D (**1**) was isolated as yellow amorphous powder. In the MS/MS spectrum of **1**, the most abundant fragment peak (m/z 373) was due to the successive loss of an H_2O and a prenyl unit C_4H_8 (56 Da). This fragment further dissociated by the loss of an H_2O and a prenyl unit C_4H_8 to produce additional fragment ions at m/z 355 and 287. These fragmentation characteristics indicated that **1** might contain two hydroxylated prenyl groups. The ^{13}C NMR and DEPT spectra showed 12 aromatic carbons (including five oxygenated), one carbonyl carbon, two oxygenated quaternary carbons, four sp^3 methylene carbons, four sp^3 methyl groups, and one methoxyl group. The 1H NMR spectrum of **1** showed a chelated hydroxyl proton signal at δ_H 13.28 (1H, s), a methoxy signal at δ_H 3.82 (3H, s), two *ortho*-coupled aromatic proton signals at δ_H 7.54 (1H, d, $J = 8.6$ Hz) and 6.93 (1H, d, $J = 8.6$ Hz), and two 3-hydroxy-3-methylbutyl moiety signals, one showing a pair of gemdimethyl signals at δ_H 1.18 (6H, s) and two methylene signals at δ_H 2.64 (2H, m) and 1.59 (2H, m). The other 3-hydroxy-3-methylbutyl group exhibited a pair of gem-dimethyl signals at δ_H 1.24 (6H, s) and two methylene signals at δ_H 2.86 (2H, m) and 1.70 (2H, m). Based on the abovementioned information, compound **1** was proposed as a xanthone bearing a methoxy group and two 3-hydroxy-3-methylbutyl groups. The locations of two 3-hydroxy-3-methylbutyl moieties and a methoxy group were assigned to C-2 (δ_C 117.3), C-4 (δ_C 114.1), and C-3 (δ_C 162.7), respectively, based on the correlations from the methoxy protons at δ_H 3.82 to C-3, from H-11 (δ_H 2.64) to C-3, C-4, and C-4a (δ_C 152.3), as well as from H-16 (δ_H 2.86) to C-1 (δ_C 157.8) and C-2 in the HMBC spectrum (Fig. 2). Furthermore, the HMBC correlations from aromatic proton at δ_H 7.54 to C-6 (δ_C 146.4), C-10a (δ_C 152.9), and C-9 (δ_C 180.8), and from aromatic proton at δ_H 6.93 to C-5 (δ_C 132.6) and C-8a (δ_C 112.5) indicated that the locations of those two *ortho*-coupled aromatic protons were C-7 (δ_C 113.4) and C-8 (δ_C 116.2). Hence, the structure of **1** was assigned as 1,5,6-trihydroxy-3-methoxy-2,4-bis(3-hydroxy-3-methylbutyl)xanth-6-one.

The UV and NMR spectra of oblongixanthone E (**2**) were similar to those of **1**, suggesting that **2** was also a xanthone with one methoxy group and two 3-hydroxy-3-methylbutyl groups (Figures S1, S2, and Table 1).

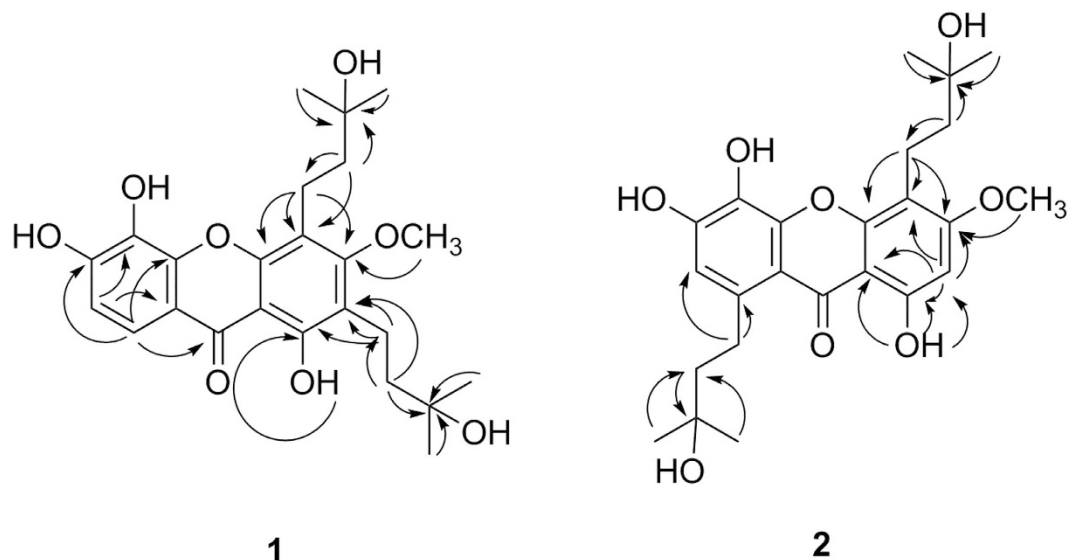


Figure 2. Key correlations observed in the HMBC NMR spectra of **1** and **2**.

No.	1 ^b		2 ^c	
	δ_H (J in Hz)	δ_C	δ_H (J in Hz)	δ_C
1		157.8		161.1
2		117.3	6.43, s	93.9
3		162.7		162.9
4		114.1		107.7
4a		152.3		152.7
5		132.6		130.6
6		146.4		151.3
7	6.93, d (8.6)	113.4	6.69, s	114.5
8	7.54, d (8.6)	116.2		136.8
8a		112.5		110.1
9		180.8		182.2
9a		113.4		102.3
10a		152.9		147.7
11	2.64, m	18.2	2.81, m	16.9
12	1.59, m	43.0	1.55, m	42.7
13		68.8		69.2
14	1.18, s	29.1	1.19, s	29.2
15	1.18, s	29.1	1.19, s	29.2
16	2.86, m	18.3	3.11, m	29.7
17	1.70, m	43.2	1.59, m	45.6
18		69.3		68.9
19	1.24, s	29.1	1.17, s	29.0
20	1.24, s	29.1	1.17, s	29.0
5-OH	13.28, s		13.62, s	
OCH ₃	3.82, s	48.6	3.88, s	56.2

Table 1. ¹H and ¹³C NMR Data (DMSO-*d*₆) for Compounds **1** and **2**^a. ^aAssignments based on DEPT, HSQC, and HMBC experiments; chemical shifts in ppm. ^bData were measured at 600 and 150 MHz. ^cData were measured at 400 and 100 MHz.

However, the MS/MS spectrum of **2** is different from that of **1** (Figures S1 and S2). Furthermore, comparison of the NMR data of **2** with those of **1** suggested that **2** is a 1,3,4,5,6,8-hexsubstituted xanthone [δ_H 6.69 (1H, s) and 6.43 (1H, s)], compared to 1,2,3,4,5,6-hexsubstituted ring system of **1** [δ_H 7.54 (1H, d, $J = 8.6$ Hz) and 6.93 (1H, d, $J = 8.6$ Hz)]. HMBC correlations between 1-OH/C-1, 1-OH/C-2, 1-OH/C-3, H-2/C-1, H-2/C-3, OCH₃/C-3, H-11/C-3, H-11/C-4, H-11/C-4a, H-16/C-7, and H-16/C-8 indicated that the locations of two 3-hydroxy-3-methylbutyl moieties, a methoxy group, and two aromatic protons were at C-4 (δ_C 107.7),

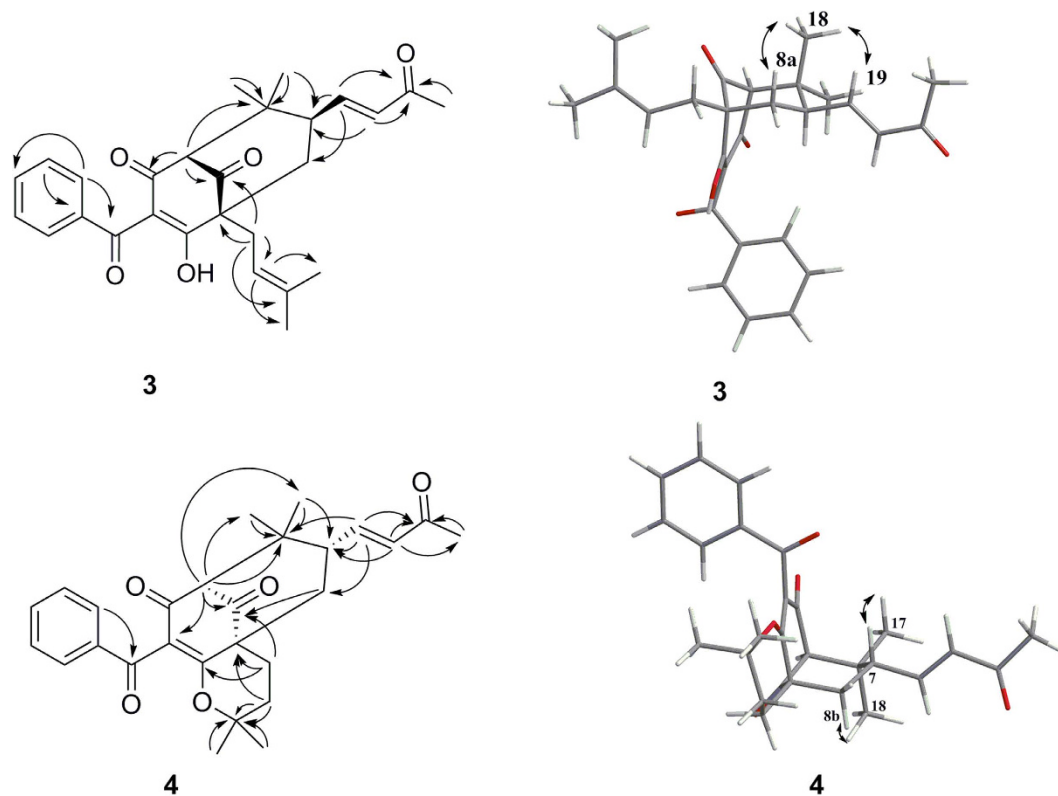


Figure 3. Key correlations observed in the HMBC and NOESY NMR spectra of **3** and **4**.

C-8 (δ_C 136.8), C-3 (δ_C 162.9), C-2 (δ_C 93.9), and C-7 (δ_C 114.5), respectively (Fig. 2). Therefore, **2** was determined to be 1,5,6-trihydroxy-3-methoxy-4,8-bis(3-hydroxy-3-methylbutyl)xanth-6-one.

Oblongifolin V (**3**) was obtained as a pale yellow gum. The molecular formula $C_{27}H_{30}O_5$ was established by HRESIMS analysis and NMR spectroscopic data. The MS/MS spectrum of **3** showed a diagnostic fragment ion at m/z 165.0182 in the positive mode, suggesting that it might be a type B PPAP with no prenyl substituent at C-5¹⁴ (Figure S3). The 1H NMR spectrum indicated the presence of a monosubstituted benzene ring [δ_H 7.56 (1H, m), 7.42 (2H, m), and 7.59 (2H, m)], an *E*-configured carbon-carbon double bond [δ_H 6.71 (1H, dd, $J = 15.7, 7.7$ Hz) and 6.16 (1H, d, $J = 15.7$ Hz)], a vinyl proton [δ_H 5.18 (1H, brs)], two methylenes [δ_H 1.94, 1.89, 2.50, and 2.44], two methines [δ_H 3.13 (1H, s), 2.67 (1H, m)], and five methyl groups [δ_H 2.65 (3H, s), 1.72 (3H, s), 1.63 (3H, s), 1.17 (3H, s), and 1.02 (3H, s)]. The ^{13}C NMR and DEPT spectra showed signals pertaining to a nonconjugated ketone (δ_C 206.8), an enolized 1,3-diketone (δ_C 196.5, 119.5, and 184.8), two quaternary carbons (δ_C 64.4 and 44.9), a methylene (δ_C 41.9), and two methines (δ_C 69.6 and 45.2), which allowed us to identify the bicyclo[3.3.1]nonane ring system typical of the prenylated benzoylphloroglucinols¹⁷. Resonances for six aromatic carbons and a conjugated carbonyl group (δ_C 198.1) were also observed, revealing the occurrence of a benzoyl group. In the HMBC spectrum, the long range correlations observed from the olefinic H-19 (δ_H 6.71, dd, $J = 15.7, 7.7$ Hz) signal to C-7 (δ_C 45.2) and C-8 (δ_C 41.9), along with correlations from olefinic H-20 (δ_H 6.16, d, $J = 15.7$ Hz) to the ketone resonance at δ_C 200.8 (C-21), which was in turn correlated with CH₃-22, established a 3-buten-2-one side chain located at C-7. Other key HMBC correlations are shown in the Fig. 3. Based on these data, compound **3** was elucidated as a prenylated benzoylphloroglucinol with a prenyl unit at C-1 (δ_C 64.4), a 3-buten-2-one side chain at C-7, and no prenyl unit at C-5 (δ_C 69.6).

The relative configuration of **3** was defined via a NOESY experiment. The correlations between H-19 (δ_H 6.71)/H-18 (δ_H 1.02) and H-8a (δ_H 1.94)/H-18 showed that the orientation of the 3-buten-2-one group at C-7 was β (Fig. 3). Thus, there were two possible isomers: (1*R*,5*R*,7*R*)-**3** and (1*S*,5*S*,7*S*)-**3**. The absolute configuration of **3** was determined by comparison of its experimentally measured electronic circular dichroism (ECD) curve with curves calculated using the TDDFT method. Consequently, the overall pattern of the calculated ECD curve of (1*R*,5*R*,7*R*)-**3** was consistent with the experimental ECD spectrum of **3** (Fig. 4). Therefore, the structure of oblongifolin V (**3**) was established as shown.

Oblongifolin W (**4**) gave the same molecular formula ($C_{27}H_{30}O_5$) as **3** (m/z 435.2173 [$M + H$]⁺ (calcd 435.2166)) by HRESIMS. Comparison of its NMR data (Table 2) with those of **3** revealed these compounds to be closely related, except for differences between C-23 (δ_C 23.4), C-24 (δ_C 30.9), C-25 (δ_C 84.8), C-26 (δ_C 29.8), and C-27 (δ_C 26.7) of **4** and C-23 (δ_C 31.2), C-24 (δ_C 120.8), C-25 (δ_C 135.8), C-26 (δ_C 26.4), and C-27 (δ_C 18.4) of **3**. This finding indicated the presence of a 2,2-dimethyl-pyran moiety in **4** instead of a 3-methylbut-2-enyl side chain in **3**. HMBC correlations between H-23/C-1, H-23/C-2, H-23/C-9, H-23/C-25, H-24/C-1, H-24/C-25, H-26/C-25, H-27/C-25, and H-27/C-24 confirmed the presence of the 2,2-dimethyl-pyran moiety fused at C-1 (δ_C 50.2) and C-2 (δ_C 174.5). Key HMBC correlations are shown in Fig. 3. The relative configuration of **4** was

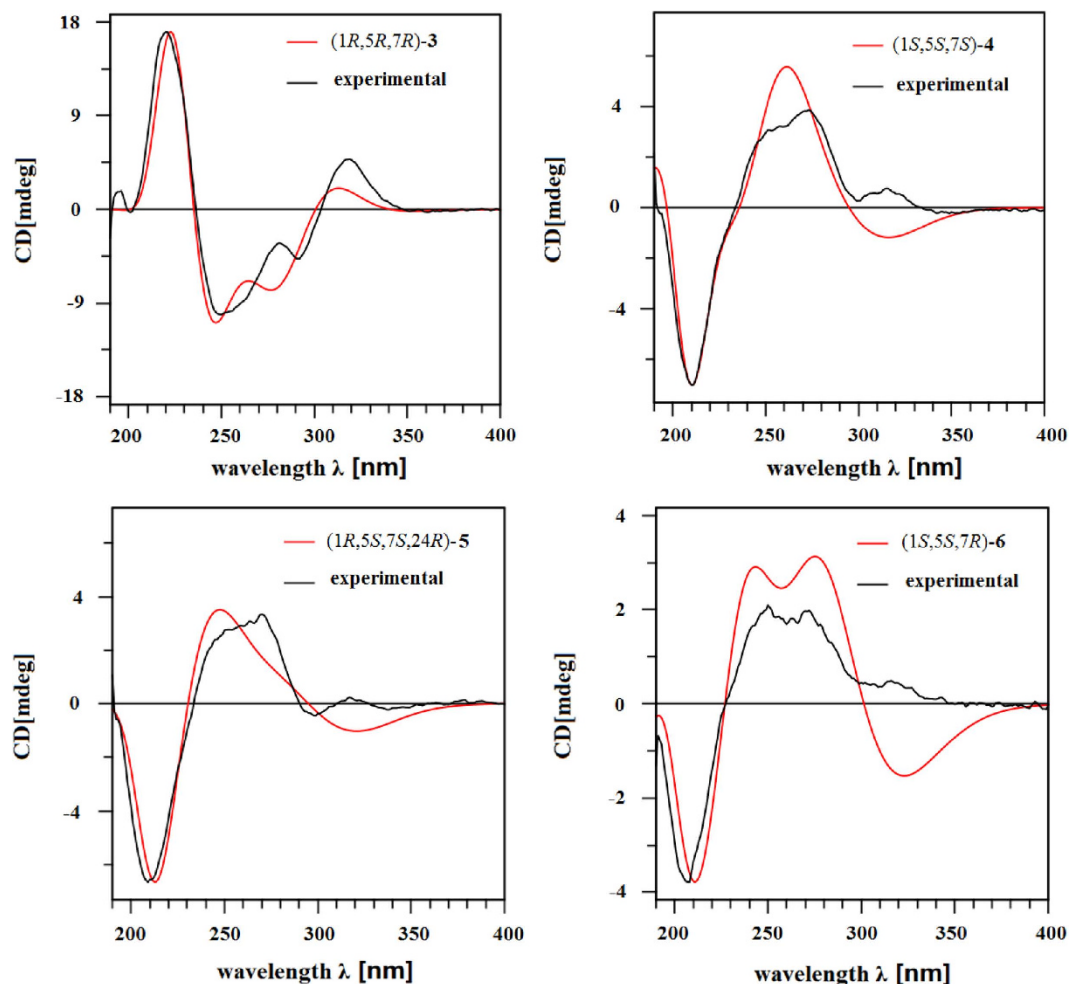


Figure 4. Calculated ECD spectra of 3–6 and their experimental curves.

assigned using NOE correlations, as shown in Fig. 3. Thus, two possible isomers, (1R,5R,7R)-4 and (1S,5S,7S)-4, were considered, and the ECD spectra were calculated. Visual inspection suggested that the (1S,5S,7S)-4 curve was similar to the experimental curve (Fig. 4). Thus, the structure of 4 was designated as shown.

The molecular formula of oblongifolin X (5) was determined to be $C_{27}H_{28}O_5$ by HRESIMS. The 1H and ^{13}C NMR data showed close similarities to those of 4, with the exception of differences at C-23 (5: δ_C 34.3, CH_2 ; 4: δ_C 23.4, CH_2), C-24 (5: δ_C 91.1, CH ; 4: δ_C 30.9, CH_2), C-25 (5: δ_C 142.5, C; 4: δ_C 84.8, C), C-26 (5: δ_C 114.9, CH_2 ; 4: δ_C 29.8, CH_3), and C-27 (5: δ_C 17.3, CH_3 ; 4: δ_C 26.7, CH_3). HMBC correlations between H-23/C-1, H-23/C-2, H-23/C-8, H-23/C-9, H-23/C-24, H-24/C-23, H-24/C-25, H-24/C-26, H-24/C-27, H-26/C-24, H-26/C-25, H-27/C-24, H-27/C-25, and H-27/C-26 confirmed the presence of a (2-isopropenyl)dihydrofuran ring moiety fused with the phloroglucinol moiety at C-1 (δ_C 61.7) and C-2 (δ_C 178.9) (Figure S14, Supplementary information). These data confirmed that a (2-isopropenyl)dihydrofuran ring moiety at C-1 and C-2 of 5 replaced the 2,2-dimethyl-pyran moiety in 4. The planar structure of 5 was further elucidated by careful interpretation of the 2D NMR experiments. The relative configuration of 5 was determined by a NOESY experiment. Key NOE correlations are shown in Figure S14. Furthermore, the calculated ECD curve (Fig. 4) for 5 led to the absolute structure being determined as shown.

Oblongifolin Y (6) was obtained as a pale yellow gum, and its molecular formula of $C_{25}H_{28}O_6$ was established by the positive HRESIMS ion at m/z 425.1969 $[M+H]^+$ (calcd for $C_{25}H_{29}O_6$, 425.1959). Comparison of the spectroscopic data of 6 with those of 4 showed that 6 is also a benzoylphloroglucinol with a 2,2-dimethyl-pyran moiety fused to the phloroglucinol moiety at C-1 and C-2. The only structural difference between the two compounds was the presence of an acetoxy group ($COOH-CH_2-$) in 6 instead of the 3-buten-2-one group in 4. The location of the acetoxy group was assigned to C-7 by the HMBC correlations from H-7 (δ_H 2.74) to C-19 (δ_C 34.3), as well as H-19 (δ_H 2.65) to C-20 (δ_C 173.9). The structure of 6 was confirmed by DEPT, HSQC, HMBC, and NOESY experiments. The key HMBC and NOE correlations are shown in Figure S15 (Supplementary information). Furthermore, an ECD experiment and ECD calculation of 6 were conducted. The experimental ECD spectrum of 6 was consistent with the calculated ECD spectra for (1S,5S,7R)-6 (Fig. 4), thus establishing the assignment of the absolute configuration of 6 as depicted.

Oblongifolin Z (7) was obtained as a pale yellow gum. The molecular formula $C_{33}H_{44}O_5$ for 7 was calculated from the HREIMS of the ion peak $[M+Na]^+$ m/z 543.3083 (calc. 543.3081). The 1H NMR data of this compound

Position	3 ^b		4 ^b		5 ^b		6 ^c	
	δ_{H} (J in Hz)	δ_{C}	δ_{H} (J in Hz)	δ_{C}	δ_{H} (J in Hz)	δ_{C}	δ_{H} (J in Hz)	δ_{C}
1		64.4		50.2		61.7		50.1
2		196.5		174.5		178.9		172.7
3		119.5		126.6		118.3		126.6
4		184.8		193.1		193.1		191.6
5	3.13, s	69.6	3.00, s	74.9	2.98, s	74.1	2.87, s	75.2
6		44.9		43.6		44.2		42.8
7	2.67, m	45.2	2.93, m	45.0	2.94, m	45.2	2.74, m	37.7
8	1.94, m	41.9	2.43, dd (14.0, 4.6)	38.6	2.40, dd (14.1, 4.8)	37.2	2.62, m;	39.4
	1.89, m		1.91, m		2.21, m		1.61, t (13.1)	
9		206.8		205.7		202.8		205.7
10		198.1		196.1		194.2		193.9
11		139.2		138.6		138.3		138.6
12	7.59, m	130.0	7.84, m	130.2	7.79, m	130.4	7.95, d (7.4)	129.9
13	7.42, m	129.3	7.52, m	130.0	7.50, m	130.0	7.50, t (7.6)	129.6
14	7.56, m	134.0	7.65, m	135.2	7.63, m	135.3	7.60, t (7.3)	134.1
15	7.42, m	129.3	7.52, m	130.0	7.50, m	130.0	7.50, t (7.6)	129.6
16	7.59, m	130.0	7.84, m	130.2	7.79, m	130.4	7.95, d (7.4)	129.9
17	1.17, s	27.9	1.09, s	27.5	1.13, s	27.6	1.09, s	26.8
18	1.02, s	21.6	0.98, s	21.3	1.02, s	21.5	0.91, s	20.7
19	6.71, dd (15.7, 7.7)	146.9	6.83, dd (15.9, 8.4)	146.3	6.83, dd (15.9, 8.3)	146.1	2.65, m	34.3
							2.18, m	
20	6.16, d (15.7)	134.5	6.30, d (15.9)	134.7	6.28, d (15.9)	134.7		173.9
21		200.8		200.7		200.8	2.45, m	23.1
							1.71, m	
22	2.65, s	26.4	2.31, s	27.5	2.29, s	27.5	2.03, m	30.8
							1.83, m	
23	2.50, m;	31.2	2.53, m;	23.4	2.59, dd (13.2, 11.2)	34.3		83.2
	2.44, m		1.79, m		2.21, m			
24	5.18, brs	120.8	2.07, m	30.9	5.39, dd (11.2, 5.3)	91.1	1.23, s	29.9
			1.80, m					
25		135.8		84.8		142.5	1.09, s	26.3
26	1.72, s	26.4	1.27, s	29.8	4.93, m	114.9		
27	1.63, s	18.4	0.99, s	26.7	1.60, s	17.3		

Table 2. ¹H and ¹³C NMR Data (600 and 150 MHz) for Compounds 3–6^a. ^aAssignments based on DEPT, HSQC, HMBC, and NOESY experiments; chemical shifts in ppm. ^bMeasured in CD₃OD/0.1% TFA. ^cMeasured in acetone-*d*₆.

were similar to values obtained for the known compound oblongifolin Q³, except for differences between H-30 [δ_{H} 1.44 (1H, m) and 1.34 (1H, m)] and H-32 [δ_{H} 1.12 (3H, s)] in 7 and H-30 [δ_{H} 3.95 (1H, t, $J = 6.1$ Hz)] and H-32 [δ_{H} 4.89 (1H, s) and 4.80 (1H, s)] in oblongifolin Q. This information indicated the occurrence of a 3-hydroxy-3-methylbutyl group at C-23 in 7 instead of the 2-hydroxy-3-methylbutenyl group of oblongifolin Q. This conclusion was further confirmed by the ¹³C NMR data of C-29 (δ_{C} 23.5, CH₂), C-30 (δ_{C} 44.3, CH₂), C-31 (δ_{C} 71.6, C), and C-33 (δ_{C} 29.29, CH₃) and HMBC correlations between H-30/C-33, H-32/C-30, H-32/C-31, H-32/C-33, H-33/C-30, H-33/C-31, and H-33/C-32 (Figure S16, Supplementary information). According to the observed NOE correlations (Figure S16), the relative configuration of 7 was deduced to be the same as those of oblongifolin Q. In addition, the experimental ECD spectrum of 7 was consistent with that of 7 (Figure S17), suggesting that the absolute configuration of 7 is the same as that of oblongifolin Q. Thus, the structure of oblongifolin Z (7) was established as shown.

Oblongifolin AA (8) had the same molecular formula as the known compound 9 (C₃₃H₄₄O₄), which was deduced from HRESIMS. The MS/MS spectrum of 8 in positive was also in near agreement with that of 9 (Figure S18, Supplementary information). The ¹H and ¹³C NMR data (Table 3) showed close similarities to those of 9, with the exception of significant differences in the chemical shifts at C-7, C-8, C-17, and C-18 due to the opposite configuration of C-7 [δ_{C} 45.5, 41.0, 25.4, and 31.5 for 8, respectively, versus δ_{C} 42.4, 43.2, 27.6, and 21.2 for oblongifolin L, respectively]. These data indicated that 8 was a C-7 epimer of oblongifolin L. The structure of 8 was confirmed by DEPT, HSQC, HMBC, and NOESY experiments. The absolute configuration of 8 was also assigned by experimental and theoretically calculated ECD methods. As shown in Figure S19, the absolute configuration of 8 was determined as shown.

Position	7		8	
	δ_{H} (J in Hz)	δ_{C}	δ_{H} (J in Hz)	δ_{C}
1		65.3		63.2
2		197.2		196.9
3		119.0		117.1
4		185.3		188.5
5	3.08, s	70.1	3.03, s	68.3
6		45.4		46.3
7	1.74 m	42.5	1.55, m	45.5
8	2.02, m; 1.48, m	43.1	2.21, m; 2.18, m	41.0
9		207.6		208.8
10		198.1		197.9
11		139.1		139.0
12	7.59, m	129.9	7.55, m	129.9
13	7.41, m	129.2	7.41, m	129.2
14	7.55, m	133.9	7.55, m	133.9
15	7.41, m	129.2	7.41, m	129.2
16	7.59, m	129.9	7.55, m	129.9
17	1.24, s	27.5	1.28, s	25.4
18	0.99, s	21.2	1.17, s	31.5
19	2.17, m; 1.74, m	28.9	2.21, m; 2.08, m	30.4
20	5.06, m	124.0	4.90, m	125.1
21		138.3		137.8
22	1.58, s	16.3	1.57, s	16.4
23	1.98, m	41.3	2.04, m; 1.96, m	41.0
24	2.44, m	31.3	2.47, dd (13.9, 8.6)	31.7
	2.38, m		2.35, dd (13.7, 5.5)	
25	5.17, m	121.1	5.21, t (6.3)	120.9
26		135.5		135.7
27	1.72, s	26.4	1.72, s	26.4
28	1.61, s	18.4	1.62, s	18.4
29	1.45, m; 1.35, m	23.5	2.07, m; 1.97, m	27.7
30	1.44, m; 1.34, m	44.3	5.06, t (6.8)	125.5
31		71.6		132.3
32	1.12, s	29.27	1.65, s	25.1
33	1.12, s	29.29	1.57, s	18.4

Table 3. ^1H and ^{13}C NMR Data (400 and 100 MHz, $\text{CD}_3\text{OD}/0.1\%$ TFA) for Compounds 7 and 8.

^aAssignments based on DEPT, HSQC, HMBC, and NOESY experiments; chemical shifts in ppm.

Compounds 1, 2, and 9 inhibit migration in TE1 cells. Our previous studies showed that compounds isolated from *Garcinia* species had potent inhibitory effect on esophageal cancer cell metastasis^{10,18}. In addition, the EtOAc-soluble fraction of the actone extract of *G. oblongifolia* leaves could inhibit TE1 cell migration at concentrations of 12.5, 25 and 50 $\mu\text{g}/\text{ml}$ (Figure S20). Therefore, all isolates were screened by wound healing assay to identify new compounds with anti-metastasis activity in esophageal cancer cells. As shown in Fig. 5, after treatment with various compounds at a concentration of 20 μM , compared to the positive control sorafenib (SFB), compounds 1, 2, and 9 exhibited the ability to inhibit migration in TE1 cells. The cell cytotoxicity tested by MTT assay showed that all compounds had lower cytotoxicity in TE1, KYSE150, HepG2, A549, and HL7702 cell lines (Table S1, Supplementary information). Moreover, the results indicated that TE1 cells were more sensitive to 1, 2 and 9 than other cells.

Transwell assay was performed to confirm the effect of all isolates on cell migration. After being incubated with these compounds at 10 and 20 μM for 24 h, TE1 cells were fixed and imaged, and the number of migrated cells was counted. As shown in Fig. 6, the migrated cells were significantly reduced after compounds 1, 2 and 9 treatments. Statistical data also suggested that 1, 2 and 9 could significantly inhibit cell migration. In addition, compounds 3–8 had no significant effect on cell migration, which was consistent with the results of wound healing assay (Figure S21). A transwell invasion assay was performed to investigate whether the invasion ability was blocked by 1, 2 and 9. The results suggested that 9 significantly attenuated TE1 cells invasion. Moreover, compounds 1 and 2 did not inhibit cell invasion in the matrigel invasion assay (Figure S22, Supplementary information). All these results suggest that 1, 2 and 9 showed a potential effect on cell metastasis.

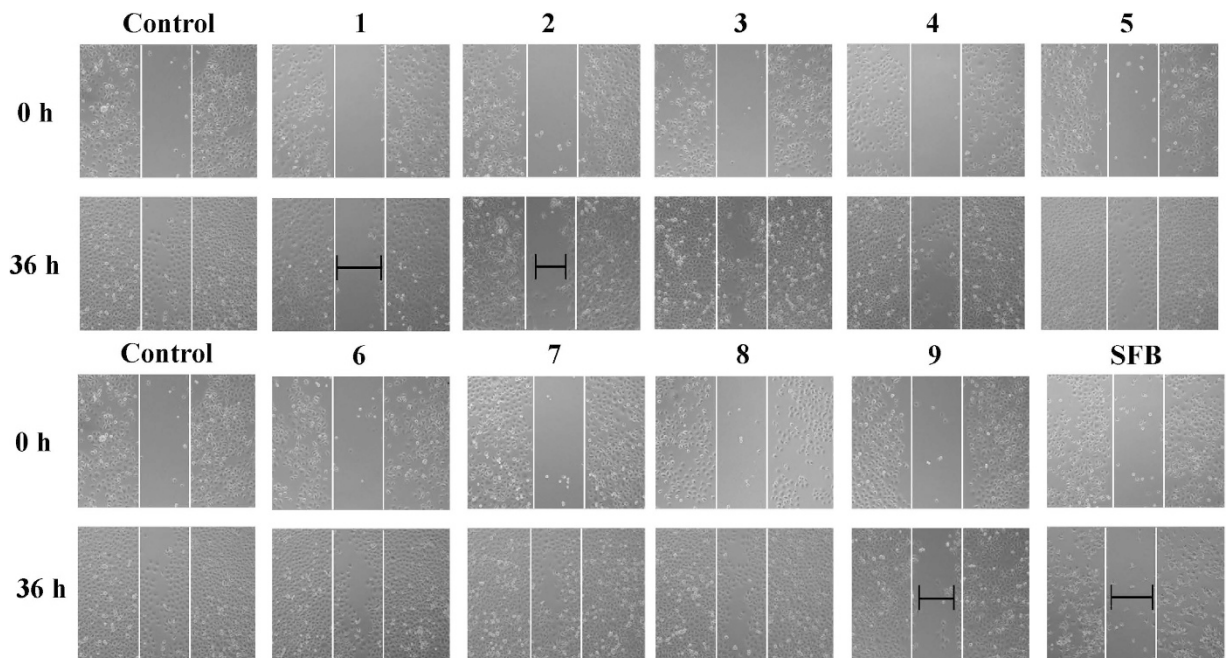


Figure 5. Anti-migration effect of compounds on human esophageal carcinoma cells (TE1) by wound healing assay. TE1 cells monolayer was scratched and treated with isolates at concentration of $20\mu\text{M}$. Sorafenib (SFB) was used as the positive control. Images were accessed by a microscope.

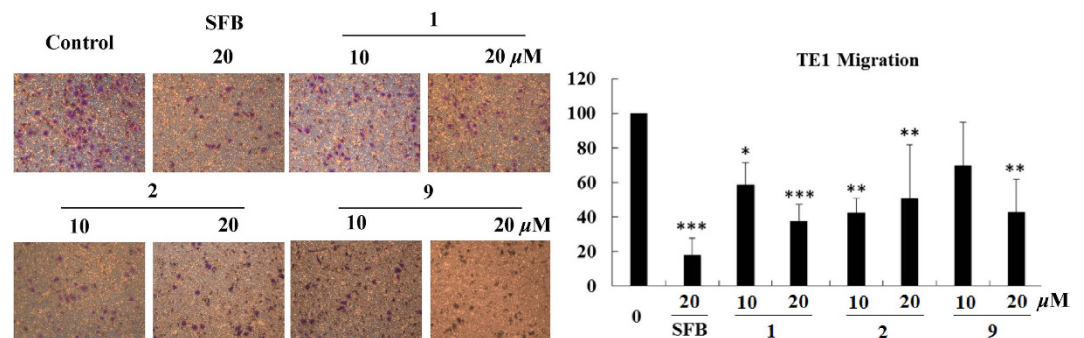


Figure 6. Compounds 1, 2, and 9 inhibit migration in TE1 cells measured by transwell assay. Cells were incubated with 1, 2, or 9 for 36 h, and migrated cells were fixed and stained with 0.1% crystal violet. Sorafenib (SFB) was used as the positive control. The summary data for transwell migration assay were presented as the means \pm S.D. * $P < 0.05$, ** $P < 0.01$, *** $P < 0.001$.

Compounds 1, 2, and 9 downregulate RAF-MAPK signaling pathway and snail protein level. The RAF-MEK-ERK cascade plays a central role in the regulation of cell metastasis, proliferation and survival. The high frequency of this pathway deregulated in human cancer makes it an attractive target for drug development¹⁹. Therefore, we examined whether these compounds with anti-metastasis activity could interfere RAF-MAPK cascades. Western blot showed that the 24 h treatment of 1, 2, and 9 attenuated BRAF and CRAF protein levels at both 10 and $20\mu\text{M}$ (Fig. 7). In addition, compounds 2 and 9 inhibited phospho-MEK and phospho-ERK, suggesting that these two compounds could also interfere downstream signals. No significant changes were detected on RAS, MEK and ERK proteins (Fig. 7), as well as on BRAF and CRAF mRNA levels (Figure S22, Supplementary information).

The epithelial-mesenchymal transition (EMT) is a fundamental process that acts on ending cells with migratory and invasive properties. Snail is a protein that promotes EMT, acting as an EMT marker²⁰. To illustrate whether these compounds could affect snail protein, we performed a western blot analysis. The results showed that 1, 2, and 9 reduced snail protein (Fig. 7), suggesting that they could regulate the EMT pathway. In conclusion, compounds 1, 2, and 9 could downregulate the RAF-MEK-ERK cascades and regulate EMT pathway by decreasing snail protein, indicating that these compounds could inhibit cell migration through multiple signaling pathways.

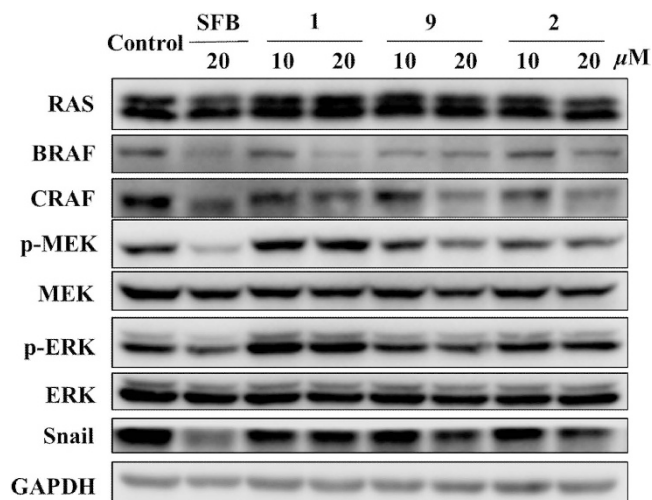


Figure 7. Compounds 1, 2, and 9 downregulate RAF-MAPK signaling pathway and snail protein level. RAS-RAF-MEK-ERK cascades and snail protein were analyzed by western blot. TE1 cells were treated with 1, 2, or 9 with various concentrations (0, 10, 20 μM) for 48 h. Sorafenib (SFB) was used as the positive control.

Experimental Section

General Experimental Procedures. Optical rotations were measured using an Autopol VI polarimeter. Ultraviolet absorption spectra were recorded on a UV-2401 PC spectrophotometer. ECD spectra were recorded on a Chirascan-plus spectrometer (Applied photophysics Ltd., Surrey, United Kingdom). IR spectra were obtained from a Perkin-Elmer 577 spectrometer. NMR spectra were measured on a Bruker AV-600 or AV-400 spectrometer and calibrated by the solvent peak used. Mass spectrometry was performed on a SYNAPT G2-Si HDMS (Waters Corp., Manchester, UK) with an electrospray ion source (Waters, Milford, MA) connected to a lock-mass apparatus, which performed real-time calibration correction. Column chromatography was performed with CHP20P MCI gel (75–150 μm , Mitsubishi Chemical Corporation, Japan), silica gel (100–200, or 200–300 mesh, Qingdao Haiyang Chemical Co., Ltd.), Sephadex LH-20 (GE Healthcare Bio-Sciences AB, Sweden), and reversed-phase C_{18} silica gel (50 μm , YMC, Kyoto, Japan). Precoated TLC sheets of silica gel 60 GF254 (Qingdao Haiyang Chemical Co., Ltd.) were used. A Waters 2535 Series machine equipped with a Xbridge C_{18} column (4.6 \times 250 mm, 5 μm) was used for HPLC analysis, and a preparative Xbridge Prep C_{18} OBD column (19 \times 250 mm, 5 μm) was used for the sample preparation.

Plant Material. The leaves of *G. oblongifolia* were collected at Bobai, Guangxi Zhuang Autonomous Region, People's Republic of China in December, 2005. The sample was identified by Dr. Chun-Feng Qiao. A voucher specimen (Herbarium No. 20120843) was deposited at the Engineering Research Centre of Shanghai Colleges for TCM New Drug Discovery, Shanghai University of Traditional Chinese Medicine.

Extraction and Isolation. According to the previous separation process³, the EtOAc-soluble fraction (220 g) of an acetone extract of the leaves of *G. oblongifolia* has been obtained. A UPLC-PDA-QTOFMS-guided isolation approach was employed to track the potentially new compounds during the entire isolation process. The EtOAc-soluble fraction was subjected to column chromatography (CC) on MCI, and successively eluted with H_2O , 30%, 95% EtOH, and EtOAc. The 95% EtOH-eluting fraction was separated by chromatography on a silica gel column using a gradient of petroleum ether-acetone (100:0 to 0:100, v/v) to yield 8 fractions A–K.

Fraction F (2.8 g) was subjected to reversed-phase C_{18} silica gel CC and eluted in a step gradient manner with MeOH- H_2O (60:40 to 100:0) to obtain fifteen subfractions Fa–Fp. Subfraction Fb was purified by preparative HPLC (MeCN- H_2O , 45:55, with 0.1% formic acid in H_2O , 20 ml/min) to yield compound 3 (12.5 mg). Subfraction Fd was further separated by preparative HPLC (MeCN- H_2O , 39:61, with 0.1% formic acid in H_2O , 20 mL/min) to give compounds 4 (7.1 mg) and 5 (2.7 mg). Compounds 8 (27.3 mg) and 9 (50 mg) were purified by preparative HPLC (MeCN- H_2O , 77:23, with 0.1% formic acid in H_2O , 20 ml/min) from subfraction Fo. Subfraction H (1.2 g) was subjected to CC on a reversed-phase C_{18} silica gel eluted with MeOH- H_2O in a gradient (40:60 to 100:0) to obtain 10 subfractions (Ha–Hj). Subfraction Hd was purified by preparative HPLC (MeCN- H_2O , 40:60, with 0.1% formic acid in H_2O , 20 ml/min) to yield compound 7 (8.1 mg). Fraction I (1.2 g) was chromatographed on a Sephadex LH-20 column (MeOH) to obtain 9 subfractions Ia–Ii. Fraction Ib (750 mg) was subjected to reversed-phase C_{18} silica gel CC and eluted in a step gradient manner with MeOH- H_2O (50:50 to 100:0) to obtain subfractions Iba–Ibj. Subfractions Ibb, Ibc, and Ibd were purified by preparative HPLC to yield compounds 6 (5.8 mg), 1 (5 mg), and 2 (8.9 mg), respectively.

Oblongixanthone D (1): light yellow powder; UV (MeOH) λ_{max} (log ϵ) 256 (3.68), 328 (3.19) nm; IR (KBr) ν_{max} 3423, 2965, 2927, 1633, 1590, 1515, 1459, 1432, 1301, 1213, 1110, 1037, 755 cm^{-1} ; ^1H NMR (DMSO- d_6 , 600 MHz) data, see Table 1; ^{13}C NMR (DMSO- d_6 , 150 MHz) data, see Table 1; HRESIMS 447.2013 [$\text{M} + \text{H}$]⁺ (calcd for $\text{C}_{24}\text{H}_{31}\text{O}_8$, 447.2013).

Oblongixanthone E (2): light yellow powder; UV (MeOH) λ_{\max} (log ϵ) 255 (3.77), 330 (3.39) nm; IR (KBr) ν_{\max} 3428, 2965, 1646, 1523, 1444, 1384, 1321, 1115, 1105 cm^{-1} ; ^1H NMR (DMSO- d_6 , 400 MHz) data, see Table 1; ^{13}C NMR (DMSO- d_6 , 100 MHz) data, see Table 1; HRESIMS 447.2015 $[\text{M} + \text{H}]^+$ (calcd for $\text{C}_{24}\text{H}_{31}\text{O}_6$, 447.2013).

Oblongifolin V (3): light brown gum; $[\alpha]_D^{25}$ 4.3 (c 0.02, MeOH); UV (MeOH) λ_{\max} (log ϵ) 202 (4.10) nm; ECD (c 4.37×10^{-4} M, MeOH) λ_{\max} nm ($\Delta\epsilon$) 220 (+22.98), 250 (-10.10), 291 (-4.75), 319 (+4.83); IR (KBr) ν_{\max} 3359, 2921, 2850, 1722, 1633, 1590, 1573, 1467, 1382, 1280, 1025, 701 cm^{-1} ; ^1H NMR ($\text{CD}_3\text{OD}/0.1\%$ TFA, 600 MHz) data, see Table 2; ^{13}C NMR ($\text{CD}_3\text{OD}/0.1\%$ TFA, 150 MHz) data, see Table 2; HRESIMS 435.2169 $[\text{M} + \text{H}]^+$ (calcd for $\text{C}_{27}\text{H}_{31}\text{O}_5$, 435.2166).

Oblongifolin W (4): light brown gum; $[\alpha]_D^{25}$ 20.0 (c 0.03, MeOH); UV (MeOH) λ_{\max} (log ϵ) 253 (3.51) nm; ECD (c 2.42×10^{-4} M, MeOH) λ_{\max} nm ($\Delta\epsilon$) 211 (-7.03), 273 (+3.87), 315 (+0.76); IR (KBr) ν_{\max} 3359, 3197, 2956, 2923, 2852, 1733, 1677, 1633, 1596, 1467, 1365, 1233, 1118, 755 cm^{-1} ; ^1H NMR ($\text{CD}_3\text{OD}/0.1\%$ TFA, 600 MHz) data, see Table 2; ^{13}C NMR ($\text{CD}_3\text{OD}/0.1\%$ TFA, 150 MHz) data, see Table 2; HRESIMS 435.2173 $[\text{M} + \text{H}]^+$ (calcd for $\text{C}_{27}\text{H}_{31}\text{O}_5$, 435.2166).

Oblongifolin X (5): light brown gum; $[\alpha]_D^{25}$ -11.8 (c 0.03, MeOH); UV (MeOH) λ_{\max} (log ϵ) 253 (3.80) nm; ECD (c 11.76×10^{-4} M, MeOH) λ_{\max} nm ($\Delta\epsilon$) 209 (-6.64), 270 (3.34); IR (KBr) ν_{\max} 3444, 2929, 1733, 1677, 1623, 1448, 1365, 1288, 1207, 1139, 1027 cm^{-1} ; ^1H NMR ($\text{CD}_3\text{OD}/0.1\%$ TFA, 600 MHz) data, see Table 2; ^{13}C NMR ($\text{CD}_3\text{OD}/0.1\%$ TFA, 150 MHz) data, see Table 2; HRESIMS 433.2010 $[\text{M} + \text{H}]^+$ (calcd for $\text{C}_{27}\text{H}_{29}\text{O}_5$, 433.2009).

Oblongifolin Y (6): light brown gum; $[\alpha]_D^{25}$ 24.1 (c 0.06, MeOH); UV (MeOH) λ_{\max} (log ϵ) 253 (3.40) nm; ECD (c 3.54×10^{-4} M, MeOH) λ_{\max} nm ($\Delta\epsilon$) 207 (-3.78), 272 (3.39); IR (KBr) ν_{\max} 3444, 2967, 1733, 1644, 1594, 1452, 1375, 1336, 1118 cm^{-1} ; ^1H NMR (acetone- d_6 , 600 MHz) data, see Table 2; ^{13}C NMR (acetone- d_6 , 150 MHz) data, see Table 2; HRESIMS 425.1969 $[\text{M} + \text{H}]^+$ (calcd for $\text{C}_{25}\text{H}_{29}\text{O}_6$, 425.1959).

Oblongifolin Z (7): light brown gum; $[\alpha]_D^{25}$ -23.5 (c 0.03, MeOH); UV (MeOH) λ_{\max} (log ϵ) 244 (3.35), 282 (3.37) nm; ECD (c 2.60×10^{-4} M, MeOH) λ_{\max} nm ($\Delta\epsilon$) 215 (4.97), 253 (-3.74), 319 (1.63); IR (KBr) ν_{\max} 3444, 2929, 1718, 1670, 1635, 1590, 1573, 1382, 1078 cm^{-1} ; ^1H NMR ($\text{CD}_3\text{OD}/0.1\%$ TFA, 400 MHz) data, see Table 3; ^{13}C NMR ($\text{CD}_3\text{OD}/0.1\%$ TFA, 100 MHz) data, see Table 3; HRESIMS 543.3083 $[\text{M} + \text{Na}]^+$ (calcd for $\text{C}_{33}\text{H}_{44}\text{O}_5\text{Na}$, 543.3081).

Oblongifolin AA (8): light brown gum; $[\alpha]_D^{25}$ -36.2 (c 0.05, MeOH); UV (MeOH) λ_{\max} (log ϵ) 253 (3.54), 286 (3.56) nm; ECD (c 2.60×10^{-4} M, MeOH) λ_{\max} nm ($\Delta\epsilon$) 217 (21.85), 254 (-12.88), 316 (5.52); IR (KBr) ν_{\max} 3444, 2962, 2923, 1729, 1673, 1637, 1590, 1573, 1448, 1382, 1286, 1025 cm^{-1} ; ^1H NMR ($\text{CD}_3\text{OD}/0.1\%$ TFA, 400 MHz) data, see Table 3; ^{13}C NMR ($\text{CD}_3\text{OD}/0.1\%$ TFA, 100 MHz) data, see Table 3; HRESIMS 503.3167 $[\text{M} + \text{H}]^+$ (calcd for $\text{C}_{33}\text{H}_{45}\text{O}_4$, 503.3167).

UPLC-PDA-QTOFMS analysis. UPLC was performed using a Waters Acquity UPLC Iclass system (Waters, Milford, MA, USA), equipped with a binary solvent delivery system, an autosampler, and a photodiode-array detection (PDA) system. Chromatography was performed on a Waters ACQUITY BEH C_{18} column (2.1 mm \times 100 mm I.D., 1.7 μm , Waters, Milford, MA, USA). The mobile phase consisted of (A) 0.1% formic acid in water and (B) ACN containing 0.1% formic acid. The 0.1% formic acid was added to both the aqueous solution and ACN. The UPLC eluting conditions were as follows: 32–42% B (0–5 min), 42–46% B (5–10 min), 46–70% B (10–23 min), 70–95% B (23–29 min) and 95–100% B (29–32 min). The flow rate was maintained at 0.4 ml/min. The column and autosampler were maintained at 40 $^\circ\text{C}$ and 10 $^\circ\text{C}$, respectively.

Mass spectra were obtained using a SYNAPT G2-Si HDMS (Waters Corp., Manchester, UK) equipped with an electrospray ionization source. ESI mass spectra were acquired over the m/z 50–1200 range. The desolvation gas was set to 800 L h^{-1} at temperature of 400 $^\circ\text{C}$, the cone gas was set to 50 L h^{-1} , and the source temperature was set to 120 $^\circ\text{C}$. The capillary voltage was set to 2500 V. Spectra were acquired in continuum and positive mode. Argon was employed as the collision gas. The SYNAPT G2-Si HDMS system was calibrated using sodium formate clusters and operated in resolution mode. Leucine enkephalin was used as a lock mass. All fractions were analyzed by UPLC-QTOFMS using the data-dependent acquisition (DDA) mode. The top five ions were selected for MS/MS from a single MS survey scan. The scan time for MS/MS was 0.1 s. The collision energy in the trap cell was ramped from 15 to 40 V. UNIFI 1.8 was used for visualization, processing, and interpretation of MS data.

Cell culture. The human esophageal cancer cell line TE1 and the KYSE150 cells were provided from Fudan University Shanghai Cancer Center. The human cell line HepG2, A549 and HL7702 cells were purchased from the Shanghai Institute of Biochemistry and Cell Biology (Shanghai, China). Cells were grown in RPMI 1640 or DMEM medium (Hyclone, Logan, UT, USA) with 10% fetal bovine serum (FBS), 100 U/ml penicillin and 100 mg/ml streptomycin, cultivated at 37 $^\circ\text{C}$ containing 5% CO_2 .

Cell viability assay. The cell viability was assessed by an MTT assay. Briefly, 5×10^3 cells were seeded into a 96-well culture plate. After 24 h, cells were incubated with various compounds for 48 h. Approximately 10 μl of MTT (5 mg/ml) was added and dimethyl sulfoxide was used to dissolve the formazan crystals. The absorbance was measured at 570 nm by a microplate reader.

Wound healing assay. Cell motility was evaluated by wound healing. Briefly, 1×10^5 cells were seeded into a 24-well culture plate. When the cells grew to 80–90% confluence, a scratch was created through the cell monolayer by sterile 100 μl pipette tips, and media containing various dilutions of compounds were added. Cell migration was observed and imaged under an IX83 microscope (Olympus, Tokyo, Japan) after 36 h.

Transwell migration and invasion assay. Cell migration and invasion were estimated using transwell chambers (Corning, NY, USA) with a pore size of 8 μm . For the migration assay, 5×10^4 cells were added into the upper chamber in serum-free medium, and in the bottom chamber, 600 μL of 10% FBS medium was added. After incubating with various concentrations of compounds for 24 h, the cells on the upper surface of the chamber were removed using cotton swabs. The migrated cells on the bottom surface were fixed in 4% paraformaldehyde, stained with 0.1% crystal violet and scored under a light microscope in five random fields. For the transwell invasion assay, the upper chamber membranes were pre-incubated with matrigel (BD Biosciences, Bedford, MA, USA) for 2 hours at 37°C.

Quantitative Real-time PCR. After treatment, total RNA was extracted from TE1 cells using Trizol (Takara, Shiga, Japan). Then, RNA was reverse transcribed by a PrimeScript RT reagent kit. Quantitative PCR was conducted with forward and reverse primers containing SYBER Green. Then, real-time PCR was performed under a StepOnePlus Real-Time PCR System. The primers for human genes were as follows: for GAPDH, forward primer: 5'-TGTTGCCATCAATGACCCCTT-3', reverse primer: 5'-CTCCACGACGTACTCAGCG-3', for B-RAF, forward primer: 5'-CATTGGTTTTGATGAGTATATGAAC-3', reverse primer: 5'-GGAGACACTTTGTAGCAGAG-3' and for C-RAF, forward primer: 5'-TGAGCACTGTAGCACCAAAGTACCT-3', reverse primer: 5'-CAGACTCTCGCATACGACGCAT-3'.

Western blot analysis. TE1 cells were seeded on a 3.5-cm dish, treated with various compounds, and lysed in RIPA buffer. Proteins were separated on SDS polyacrylamide gels and transferred to PVDF membranes (Millipore, Billerica, MA, USA). The membranes were blocked and immunoblotted with primary antibodies at 4°C overnight, followed by appropriate secondary antibodies. GAPDH was used as the loading control. Membranes were visualized under an Image Quant LAS 4000 mini and processed by Image Quant TL 1D software (General Electric Company).

The primary antibodies C-RAF (Cat.9422), MEK1/2 (Cat.9122), p-MEK (Ser217/221, Cat.9154), ERK (Cat.4695), p-ERK (Tyr202/Tyr384, Cat.4370), GAPDH (Cat.5174) and snail (Cat.3879) were purchased from Cell Signaling Technologies (Danvers, MA, USA). RAS (Cat.ab137739) and B-RAF (Cat.ab33899) were purchased from Abcam (Cambridge, UK).

References

- Fu, W. M. *et al.* Heat shock protein 27 mediates the effect of 1,3,5-trihydroxy-13,13-dimethyl-2H-pyran [7,6-b] xanthone on mitochondrial apoptosis in hepatocellular carcinoma. *J. Proteomics* **75**, 4833–4843 (2012).
- Wu, X., Ke, C.-Q., Yang, Y.-P. & Ye, Y. New Biphenyl Constituents from *Garcinia oblongifolia*. *Helv. Chim. Acta* **91**, 938–943 (2008).
- Zhang, H. *et al.* Prenylated Benzoylphloroglucinols and Xanthenes from the Leaves of *Garcinia oblongifolia* with Antitumor Activity. *J. Nat. Prod.* **77**, 1037–1046 (2014).
- Shan, W.-G., Lin, T.-S., Yu, H.-N., Chen, Y. & Zhan, Z.-J. Polyprenylated Xanthenes and Benzophenones from the Bark of *Garcinia oblongifolia*. *Helv. Chim. Acta* **95**, 1442–1448 (2012).
- Huang, S. X. *et al.* Bioassay-guided isolation of xanthenes and polycyclic prenylated acylphloroglucinols from *Garcinia oblongifolia*. *J. Nat. Prod.* **72**, 130–135 (2009).
- Hamed, W. *et al.* Oblongifolins A-D, polyprenylated benzoylphloroglucinol derivatives from *Garcinia oblongifolia*. *J. Nat. Prod.* **69**, 774–777 (2006).
- Feng, S., Jiang, Y., Li, J., Qiu, S. & Chen, T. A new bixanthone derivative from the bark of *Garcinia oblongifolia*. *Nat. Prod. Res.* **28**, 81–85 (2014).
- Fu, W. M. *et al.* Apoptosis induced by 1,3,6,7-tetrahydroxyxanthone in Hepatocellular carcinoma and proteomic analysis. *Apoptosis* **17**, 842–851 (2012).
- Lao, Y. Z. *et al.* The natural compound oblongifolin C inhibits autophagic flux and enhances antitumor efficacy of nutrient deprivation. *Autophagy* **10**, 736–749, 10.4161/Auto.28034 (2014).
- Wang, X. *et al.* Oblongifolin C inhibits metastasis by up-regulating keratin 18 and tubulins. *Sci. Rep.* **5**, 10293, 10.1038/srep10293 (2015).
- Lu, Y. *et al.* Inhibitory effect of oblongifolin C on allergic inflammation through the suppression of mast cell activation. *Mol. Cell. Biochem.* **406**, 263–271 (2015).
- Wang, M. *et al.* Oblongifolin M, an active compound isolated from a Chinese medical herb *Garcinia oblongifolia*, potently inhibits enterovirus 71 reproduction through downregulation of ERp57. *Oncotarget* **7**, 8797–8808, 10.18632/oncotarget.7122 (2016).
- Xia, Z. X. *et al.* Bioassay-guided isolation of prenylated xanthenes and polycyclic acylphloroglucinols from the leaves of *Garcinia nuijiangensis*. *J. Nat. Prod.* **75**, 1459–1464 (2012).
- Zhang, H. *et al.* Diagnostic filtering to screen polycyclic polyprenylated acylphloroglucinols from *Garcinia oblongifolia* by ultrahigh performance liquid chromatography coupled with ion mobility quadrupole time-of-flight mass spectrometry. *Anal. Chim. Acta* **912**, 85–96 (2016).
- Zhou, Y. *et al.* Screening of polycyclic polyprenylated acylphloroglucinols from *Garcinia* species using precursor ion discovery (PID) scan and ultra performance liquid chromatography electrospray ionization Q-TOF tandem mass spectrometry. *J. Am. Soc. Mass Spectrom.* **20**, 1846–1850 (2009).
- Piccinelli, A. L., Campone, L., Dal Piaz, F., Cuesta-Rubio, O. & Rastrelli, L. Fragmentation pathways of polycyclic polyisoprenylated benzophenones and degradation profile of nemorosone by multiple-stage tandem mass spectrometry. *J. Am. Soc. Mass Spectrom.* **20**, 1688–1698 (2009).
- Nguyen, H. D., Trinh, B. T. D. & Nguyen, L.-H. D. Guttiferones Q-S, cytotoxic polyisoprenylated benzophenones from the pericarp of *Garcinia cochinchinensis*. *Phytochem. Lett.* **4**, 129–133, doi: 10.1016/j.phytol.2011.01.001 (2011).
- Ding, Z. *et al.* Griffipavixanthone, a dimeric xanthone extracted from edible plants, inhibits tumor metastasis and proliferation via downregulation of the RAF pathway in esophageal cancer. *Oncotarget*, doi: 10.18632/oncotarget.6484 (2015).
- Montagut, C. & Settleman, J. Targeting the RAF-MEK-ERK pathway in cancer therapy. *Cancer Lett.* **283**, 125–134 (2009).
- Smith, B. N. *et al.* Snail promotes epithelial mesenchymal transition in breast cancer cells in part via activation of nuclear ERK2. *PLoS One* **9**, e104987, doi: 10.1371/journal.pone.0104987 (2014).

Acknowledgements

This work was financially supported by the National Natural Science Foundation of China (Nos 81273403 and 81303188). We are grateful to Dr. Chun-Feng Qiao for collecting the plant material. The authors are grateful to Dr. Shuang Liang and Da-Hai He for fruitful discussions about structural elucidation.

Author Contributions

H.Z. and D.Z. contributed equally to this work. They conducted the main experiments, analyzed the data, and wrote the manuscript. Z.-J.D. and Y.-Z.L. performed the biological assay; H.-S.T. and H.-X.X. edited and polished this manuscript; H.Z. and H.-X.X. designed the experiments and commented the manuscript. All authors reviewed the manuscript.

Additional Information

Supplementary information accompanies this paper at <http://www.nature.com/srep>

Competing financial interests: The authors declare no competing financial interests.

How to cite this article: Zhang, H. *et al.* UPLC-PDA-QTOFMS-guided isolation of prenylated xanthones and benzoylphloroglucinols from the leaves of *Garcinia oblongifolia* and their migration-inhibitory activity. *Sci. Rep.* **6**, 35789; doi: 10.1038/srep35789 (2016).



This work is licensed under a Creative Commons Attribution 4.0 International License. The images or other third party material in this article are included in the article's Creative Commons license, unless indicated otherwise in the credit line; if the material is not included under the Creative Commons license, users will need to obtain permission from the license holder to reproduce the material. To view a copy of this license, visit <http://creativecommons.org/licenses/by/4.0/>

© The Author(s) 2016

SCIENTIFIC REPORTS

OPEN

Corrigendum: UPLC-PDA-QTOFMS-guided isolation of prenylated xanthenes and benzoylphloroglucinols from the leaves of *Garcinia oblongifolia* and their migration-inhibitory activity

Hong Zhang, Dan Zheng, Zhi-Jie Ding, Yuan-Zhi Lao, Hong-Sheng Tan & Hong-Xi Xu

Scientific Reports 6:35789; doi: 10.1038/srep35789; published online 21 October 2016; updated 23 December 2016

The original version of this Article contained a typographical error in the name of the author Dan Zheng, which was incorrectly given as Zheng Dan. This has now been corrected in both the PDF and HTML versions of the Article.



This work is licensed under a Creative Commons Attribution 4.0 International License. The images or other third party material in this article are included in the article's Creative Commons license, unless indicated otherwise in the credit line; if the material is not included under the Creative Commons license, users will need to obtain permission from the license holder to reproduce the material. To view a copy of this license, visit <http://creativecommons.org/licenses/by/4.0/>

© The Author(s) 2016